

Bound states in the continuum in cuprous oxide quantum wells

Angelos Aslanidis,¹ Jörg Main,^{1,*} Patric Rommel,¹ Stefan Scheel,² and Pavel A. Belov²

¹*Institut für Theoretische Physik I, Universität Stuttgart, 70550 Stuttgart, Germany*

²*Institut für Physik, Universität Rostock, Albert-Einstein-Straße 23-24, 18059 Rostock, Germany*

(Dated: February 17, 2025)

We propose a realistic semiconductor system containing bound states in the continuum (BICs) which allows for a practical realization. By varying the confinement strength of excitons in cuprous oxide quantum wells, we show that long-lived Rydberg states of the confined electron-hole pairs appear in the continuum background. The accuracy of calculations of the linewidths based on the coupled-channel Schrödinger equation with three channels and only few basis states is confirmed by a numerically exact solution employing a B-spline basis and the complex coordinate-rotation method. We argue that finite-sized cuprous oxide crystals, due to their large exciton binding energies, are a convenient platform for experimental identification of BICs.

Bound states in the continuum (BICs) [1, 2] are remarkable quantum states whose hallmark is the absence of linewidth broadening and which therefore exhibit giant nonradiative lifetimes. Bound states embedded in the continuum have been first suggested to exist by von Neumann and Wigner in the context of an open quantum system with rapidly oscillating potential [3]. One century later, they became of practical relevance [4–9] in photonics as particular solutions of the wave equation [10–14] and opened up important applications [15, 16]. However, the proposed quantum-mechanical examples of systems with BICs still fall into the category of speculative theoretical work, rather than practical realization. The theoretical setups [3, 17–19] are very hard to implement in atomic systems as they require rather challenging conditions such as a complicated form of the potential, extremely strong external magnetic field, etc. As a result, to our knowledge, so far there exists no quantum system that, under realistic conditions and at the current precision of measurements, allows one to identify BICs.

In this Letter, we propose a realistic semiconductor quantum system, which contains nontrivial BICs and which can be fabricated and studied experimentally in the near future. Trivial realizations of BICs can be easily obtained in semiconductor systems possessing a subband that differs in symmetry from lower subbands. In this case, the trivial BICs are uncoupled from the dominant decay channels of the lower subbands and thus have infinite lifetimes [20, 21]. These symmetry-protected states have already been theoretically studied by investigating the zero-linewidth states of electron-impurities in GaAs-based quantum wells (QWs) [22, 23]. By contrast, here we show the emergence of nontrivial BICs of electron-hole (eh) pairs confined in QWs. These BICs are coupled to other states, but exhibit zero linewidth broadening due to destructive interference of adjacent resonances as described by Friedrich and Wintgen [19]. We quantitatively show the appearance of the BICs and their nonzero-linewidth partner states by precise B-spline cal-

culations of the complex-rotated Hamiltonian [21, 24] for Rydberg excitons confined in cuprous oxide QWs [25]. We also provide a simple, but more approximate qualitative description of BIC formation within the coupled-channel Schrödinger equation by means of quantum defect theory (QDT) [26, 27].

The theory is applied to describe BICs of eh pairs in cuprous oxide QWs. Some of the already grown samples are hundreds of nanometers thick and thus enable one to strongly confine only very large Rydberg excitons [28–30]. However, the thinnest fabricated Cu₂O films reported recently [31] are only 20–30 nm thick and are potentially suitable for the study of lower exciton states. In practice, the detection of exciton transitions in such systems is quite complicated. In addition to the radiative broadening, the exciton states are broadened due to imperfections of the heterostructure, as well as interaction with phonons [32, 33]. Nevertheless, large exciton oscillator strengths together with zero nonradiative broadening of BICs and the suppression of other parasitic processes opens up the possibility to experimentally detect these states.

It is worth noting that cuprous oxide QWs are not the only system that potentially contains BICs. As shown previously [22], a similar Hamiltonian describes GaAs-based heterostructures with QWs and other layered structures, too. However, the binding energy of excitons in bulk GaAs is about 4 meV and, thus, the corresponding avoided crossings of resonances are less than 0.1 meV wide [34]. This significantly complicates the experimental detection of BICs in GaAs-based heterostructures. In contrast to GaAs, in cuprous oxide the large Rydberg energy of about 90 meV [35, 36], together with precise spectroscopic measurements allow one to firmly detect the splitting between the BIC and its partner state on the order of 2 meV as predicted by our calculations. We expect that BICs can be experimentally detected in other layered semiconductor systems with confined excitons having large Rydberg energies [37, 38]. The BICs will facilitate the enhancement of optical nonlinearities and allow one to improve performance of exciton devices such as exciton lasers [16].

* Email: main@itp1.uni-stuttgart.de

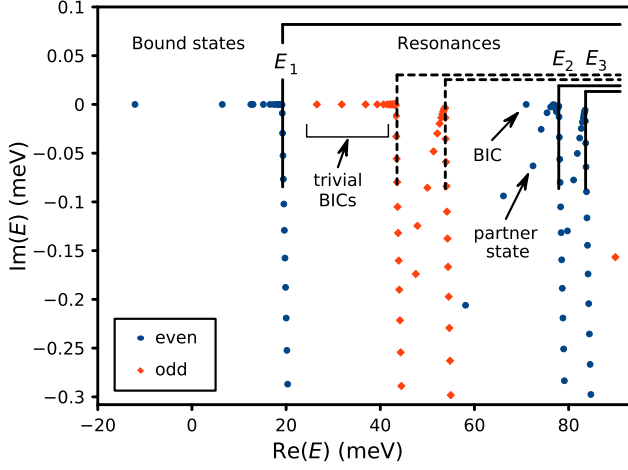


FIG. 1. Real and imaginary parts of the eh energies computed by the complex coordinate-rotation technique. The channels E_n of even parity, combining e and h quantum-confinement subbands as well as the corresponding branches of the continuum, are enumerated by the index $n = 1, 2, 3$. The bound states and resonances, including trivial (symmetry-protected) and nontrivial BICs, are explicitly denoted. The calculations were performed for a magnetic quantum number $m = 1$ and a QW width $L = 6.87$ nm for which a BIC at $E = 70.98$ meV and its partner state appear.

For the theoretical description of eh pairs in a semiconductor QW we use a hydrogenlike two-band model, as already introduced in Refs. [21, 25, 34]. The Hamiltonian

$$H(z_e, z_h, \rho) = -\frac{\hbar^2}{2m_e} \frac{\partial^2}{\partial z_e^2} + V_e(z_e) - \frac{\hbar^2}{2m_h} \frac{\partial^2}{\partial z_h^2} + V_h(z_h) - \frac{\hbar^2}{2\mu} \left(\frac{\partial^2}{\partial \rho^2} + \frac{1}{\rho} \frac{\partial}{\partial \rho} - \frac{m^2}{\rho^2} \right) - \frac{e^2}{\epsilon \sqrt{\rho^2 + (z_e - z_h)^2}} \quad (1)$$

defines two subsystems: (i) an electron confined in a QW $V_e(z_e)$ and (ii) a hole confined in a QW $V_h(z_h)$, both coupled by the screened attractive Coulomb potential with dielectric constant ϵ for both the QW and the barrier material, i.e., the Hamiltonian (1) does not consider a dielectric contrast described by the Rytova-Keldysh (RK) potential [25, 39, 40]. The kinetic operators along the z direction are defined by the effective masses m_e and m_h of electron (e) and hole (h), respectively. The cylindrical part of the energy operator is defined by the eh distance ρ in the QW plane, and describes their relative motion ($\mu = m_e m_h / (m_e + m_h)$) in this plane for a given angular harmonic specified by the magnetic quantum number m . In addition to m , the parity $\pi_z = \pi_{z_e} \pi_{z_h} = \pm 1$, related to the simultaneous exchange of $z_e \rightarrow -z_e$ and $z_h \rightarrow -z_h$, is also a good quantum number.

The resonances generated by the Hamiltonian (1) can be identified by the complex coordinate-rotation technique [24]. The rotation $\rho \rightarrow \rho \exp(i\theta)$ with an appropriate angle $\theta > 0$ converts the outgoing scattering waves (as

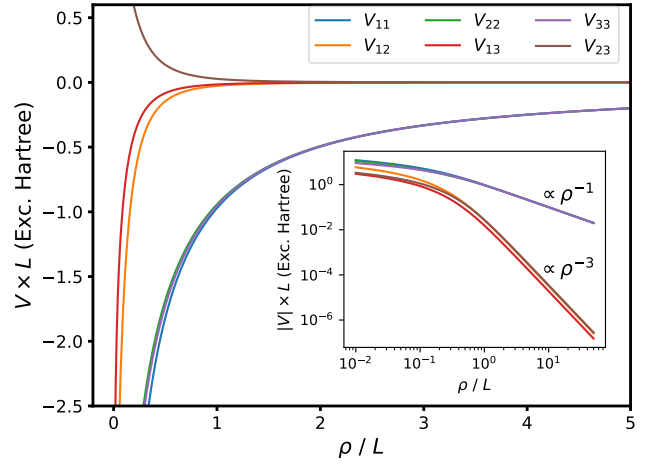


FIG. 2. Asymptotic properties of the Coulomb coupling matrix element between different quantum-confinement states. The indices correspond to the even-parity channels combining the electron and hole quantum-confinement states. The inset shows the asymptotic behavior on a double logarithmic scale. The curves for V_{22} and V_{33} visually overlap.

$\rho \rightarrow \infty$) to square-integrable functions allowing one to associate resonant states with the discrete spectrum of the non-Hermitian Hamiltonian $H(z_e, z_h, \rho \exp(i\theta))$. The artificially discretized continuum is then rotated into the complex lower half-plane by the angle 2θ . The complex energies $E - i\Gamma/2$, that are independent of the angle of rotation, give energies and linewidths of the resonances, including bound states for which $\Gamma \rightarrow 0$. The rotation along only one variable ρ is justified by the absence of scattering in the z_e and z_h directions due to the quantum-confinement barriers $V_e(z_e)$ and $V_h(z_h)$, which are taken to be large enough (or simply infinite) outside the QW of width L . Details are given in Ref. [21]. The eigenvalue problem for the complex-rotated Hamiltonian (1) was numerically solved using an expansion of the wave function over a basis of high-order B-splines [25, 41].

For a fixed QW width, the bound states, resonances, and rotated branches of the continua are shown in the complex energy plane in Fig. 1. The scattering thresholds of even parity (of e and h states) are denoted by E_n , $n = 1, 2, 3$. The energies of the excitons, i.e., the eh bound states, can be defined with respect to the sum $E_1 = E_{e1} + E_{h1}$ of the lowest energies of e and h in the confinement potentials. This sum specifies the lower boundary of the continuum, i.e., the lowest scattering threshold. Below E_1 there are only bound states of even parity, whereas above this threshold there are bound states of odd parity, the resonant states of even and odd parities. This is where potentially BICs can appear. The bound states of odd parity can be considered as trivial, symmetry-protected BICs, see Fig. 1. Above them, there are proper resonances with nonzero broadening, because their wave functions have the same parity (symmetry) as the lower subband [34] and, hence, they are coupled to

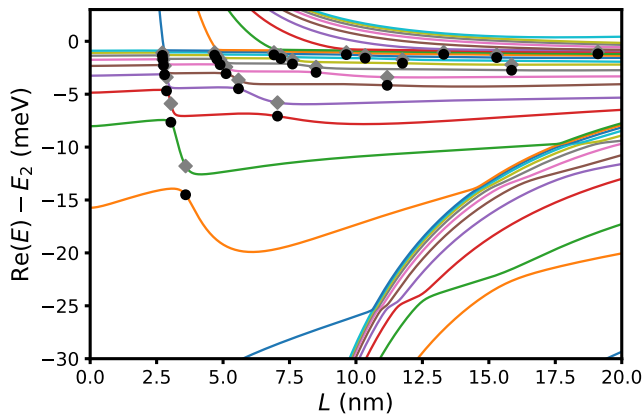


FIG. 3. Energies of the even-parity resonances with respect to the threshold E_2 as functions of the QW width L . The black circles and grey diamonds denote the BICs and their partner states, respectively.

the continuum. Among the resonances, the BIC occurring at QW width $L = 6.87$ nm and its partner state are explicitly denoted by arrows.

The resonances and BICs that appear for varying QW width L can be studied in the framework of the coupled-channel Schrödinger equation for the three lowest even-parity channels [27]

$$\left[E_n - \frac{\hbar^2}{2\mu} \left(\frac{\partial^2}{\partial \rho^2} + \frac{1}{\rho} \frac{\partial}{\partial \rho} - \frac{m^2}{\rho^2} \right) + V_{nn}(\rho) \right] \Psi_n(\rho) + \sum_{n' \neq n} V_{nn'}(\rho) \Psi_{n'}(\rho) = E \Psi_n(\rho). \quad (2)$$

The terms in square brackets in Eq. (2) represent the diagonal elements of the matrix equation. For the potentials

$$V_{nn'}(\rho) = V_{\{ij\},\{kl\}}(\rho) = -\frac{e^2}{\epsilon} \iint \frac{\psi_{ei}(z_e) \psi_{hj}(z_h) \psi_{ek}(z_e) \psi_{hl}(z_h)}{\sqrt{\rho^2 + (z_e - z_h)^2}} dz_e dz_h \quad (3)$$

we use numerically exact expansions, which is a prerequisite for the rather accurate QDT [26] results presented below. More details are given in the Supplemental Material [42]. The deviation from the exact Rydberg series originates from the non-diagonal Coulomb coupling of quantum-confinement states that are combined into channels of the same (even) parity indexed over energy from the bottom to the top by $n = \{i, j\}$, where i and j enumerate e and h single-particle states. The non-diagonal Coulomb coupling also introduces the avoided crossings of the bound states and resonances of the same parity as functions of L .

As shown in Fig. 2, the diagonal potential terms $V_{nn}(\rho)$ scale as ρ^{-1} , whereas the non-diagonal $V_{nn'}(\rho)$, with $n \neq n'$, decrease as ρ^{-3} . Therefore, asymptotically (as $\rho \rightarrow \infty$) the channels decouple. This allows one to obtain

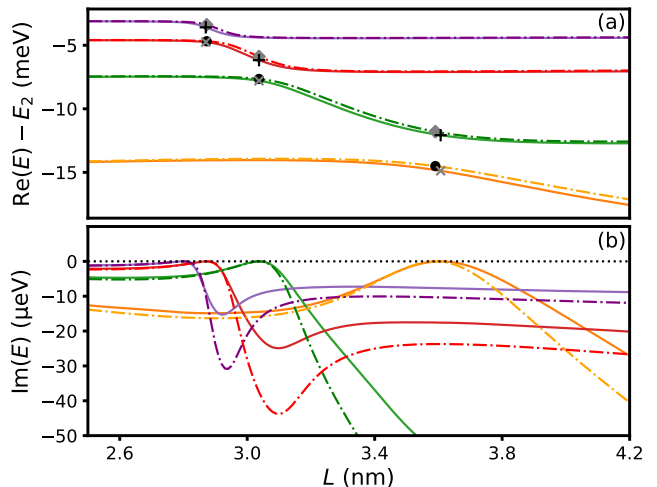


FIG. 4. Real and imaginary parts of energies of the resonances with respect to the threshold E_2 as functions of QW width L . The linewidth is $\Gamma = -2\text{Im}(E)$. The color code is the same as in Fig. 3. The solid curves show the results of complex coordinate-rotation, whereas the dashed curves are the solutions of the coupled-channel Schrödinger equation using QDT. The zero linewidths indicate the emergence of BICs.

the scattering wave functions $\Phi_1(\rho)$ in the open channel ($n = 1$) from Eq. (2) using only the diagonal potential $V_{11}(\rho)$. We use $\Phi_n(\rho)$ for the notation of the one-channel wave functions to distinguish them from the solutions $\Psi_n(\rho)$ of the coupled-channel Schrödinger equation (2), i.e., including the non-diagonal potentials.

For the two closed channels ($n = 2, 3$), the one-channel QDT wave functions $\Phi_n^N(\rho)$ with principal quantum number N are obtained as solution of the diagonal part of Eq. (2). They form a basis to set up a matrix representation of the coupled-channel Schrödinger equation, yielding the multi-channel wave functions. Details are given in the Supplemental Material [42]. With the solution of Eq. (2) at hand, the linewidth broadenings can be estimated by the Feshbach formula [22, 43]

$$\Gamma = 2\pi \left| \sum_{n=2}^3 \langle \Phi_1 | V_{1n} | \Psi_n \rangle \right|^2, \quad (4)$$

which describes the overlap of the coupling potential between the components Ψ_n , associated with the second and the third channels of the complete solution, and the regular scattering solution Φ_1 in only the first channel. It represents the interaction of the two resonances with the continuum background. The BIC appears when Γ vanishes due to destructive interference of the matrix elements in Eq. (4).

Resonant energies of the Rydberg series as a function of the QW width L are shown in Fig. 3. They are plotted with respect to the E_2 threshold. The energies of this subband tend to lie horizontally along the threshold, whereas upper (lower) subband energies are decreasing

TABLE I. Energies of the BICs and the partner states obtained from QDT and B-spline calculations. The values are given with respect to the E_2 threshold.

QDT			B-splines		
L (nm)	BIC E (meV)	partner E (meV)	L (nm)	BIC E (meV)	partner E (meV)
3.590	-14.505	-11.793	3.607	-14.875	-12.075
3.037	-7.652	-5.890	3.037	-7.793	-6.174
7.047	-7.072	-5.794	6.871	-7.362	-5.911
2.873	-4.686	-3.392	2.870	-4.754	-3.593
5.580	-4.484	-3.651	5.534	-4.614	-3.763
11.174	-4.161	-3.389	11.293	-4.418	-3.557
2.799	-3.158	-2.317	2.796	-3.199	-2.399
5.112	-3.059	-2.424	5.077	-3.132	-2.530
8.499	-2.937	-2.430	8.564	-2.673	-2.498
15.855	-2.736	-2.210	15.204	-2.549	-2.267
2.759	-2.271	-1.725	2.760	-2.297	-1.761
4.889	-2.213	-1.738	4.858	-2.260	-1.814
7.610	-2.150	-1.765	7.307	-2.217	-1.766
11.750	-2.071	-1.718	11.407	-2.179	-1.803
2.707	-1.070	-0.878	2.731	-1.729	-1.360
4.761	-1.674	-1.331	4.733	-1.706	-1.377
7.172	-1.636	-1.337	6.979	-1.680	-1.363

(increasing) as $L \rightarrow \infty$. Due to their same even parity, this subband is coupled to the continuum of subband E_1 and thus two resonances of similar energy exhibit avoided crossings as L varies. The calculated data are additionally given in Table I. Figure 4 shows in detail the dependencies on L of real and imaginary parts of several resonance energies. One observes a good agreement of the energies as well as positions of the BICs calculated by both methods: the solid curves represent the numerically exact B-spline calculations and the dashed curves are the approximate results by three-channel QDT. The agreement of the absolute values of the linewidth broadenings is more qualitative due to the limited number of channels considered for the QDT solution of Eq. (2). Nonetheless, both precise and approximate calculations show that for some values of L the imaginary parts of energies (i.e., the linewidths) vanish and BICs appear. The linewidths of the partner states also change with varying L , but they remain nonzero in the vicinity of the considered avoided crossing. Interestingly, the local maxima of linewidth broadenings of the partner states are realised not exactly at the location of the BIC, but they are slightly shifted. This fact was also noted in Ref. [8] and originates from their interaction with other resonances and subbands, complicating the problem more than when it was first discussed by Friedrich and Wintgen [19].

The idea of Friedrich and Wintgen had been that the BIC appears due to the destructive interference of two coupled resonances both in the continuum of a much lower open channel (subband). Here we give an alternative and more intuitive derivation of this effect. When restricting the QDT basis to only one state $\Phi_n^N(\rho)$ in each closed channel, those energies undergo an avoided crossing when the QW width L is varied, all calculations can

be done analytically. With E_I and E_{II} the energies of the two selected states Φ_2^I and Φ_3^{II} in the two closed channels ($n = 2, 3$), and $W = \langle \Phi_2^I | V_{23} | \Phi_3^{II} \rangle$ the matrix element of the coupling potential, the resulting (2×2) Hamiltonian matrix can be diagonalized by an orthogonal transformation, i.e.

$$O^T \begin{pmatrix} E_I & W \\ W & E_{II} \end{pmatrix} O = \begin{pmatrix} E_- & 0 \\ 0 & E_+ \end{pmatrix} \quad (5)$$

with

$$O = \begin{pmatrix} \cos \alpha & \sin \alpha \\ -\sin \alpha & \cos \alpha \end{pmatrix}. \quad (6)$$

The angle α , given by

$$\tan \alpha = \frac{1}{2W} \left[\sqrt{(E_{II} - E_I)^2 + 4W^2} - (E_{II} - E_I) \right], \quad (7)$$

defines the mixing of states and specifies the energy eigenvalues

$$E_{\pm} = \frac{1}{2} \left[(E_I + E_{II}) \pm \sqrt{(E_{II} - E_I)^2 + 4W^2} \right]. \quad (8)$$

Using the eigenvectors given by the columns of the matrix (6), the Feshbach formula (4) yields

$$\Gamma_- = \left(\sqrt{\Gamma_I} \cos \alpha - \sqrt{\Gamma_{II}} \sin \alpha \right)^2, \quad (9a)$$

$$\Gamma_+ = \left(\sqrt{\Gamma_I} \sin \alpha + \sqrt{\Gamma_{II}} \cos \alpha \right)^2, \quad (9b)$$

with $\Gamma_I = 2\pi |\langle \Phi_1 | V_{12} | \Phi_2^I \rangle|^2$ and $\Gamma_{II} = 2\pi |\langle \Phi_1 | V_{13} | \Phi_3^{II} \rangle|^2$ the linewidths of the one-channel states Φ_2^I and Φ_3^{II} . The condition for complete destructive interference of the linewidths becomes obvious from Eq. (9a): a BIC with $\Gamma_- = 0$ occurs at energy $E = E_-$ when $\tan \alpha = \sqrt{\Gamma_I / \Gamma_{II}}$. This yields the condition [19]

$$(\Gamma_{II} - \Gamma_I)W = \sqrt{\Gamma_I \Gamma_{II}} (E_{II} - E_I). \quad (10)$$

From Eqs. (9) it follows that $\Gamma_- + \Gamma_+ = \Gamma_I + \Gamma_{II}$. Thus, the partner state of a BIC with $\Gamma_- = 0$ has the linewidth $\Gamma_+ = \Gamma_I + \Gamma_{II}$, i.e., the sum of the linewidths of the two involved one-channel states.

As discussed above, the QW widths and energies of BICs in Fig. 4 and Table I obtained from QDT and the B-spline computations are in remarkably good agreement. Nevertheless, our model shows only the principal effect which may be shadowed in a real experiment due to simplifications in the Hamiltonian (1). On the one hand, the parabolic valence band of cuprous oxide is just a (first order) approximation, representing the dominant diagonal part of the Suzuki-Hensel Hamiltonian [44, 45], allowing us to use the hydrogenlike two-band model in Eq. (1). For bulk cuprous oxide the impact of the complete Suzuki-Hensel valence band structure on the yellow exciton series has been investigated both experimentally and theoretically [35, 36, 46, 47], however, to our knowledge not yet

for cuprous oxide in quantum wells. For relatively narrow QWs and for highly excited Rydberg states, the quantum confinement dominates and the effects of the complex band structure can be considered as a small perturbation [25]. On the other hand, in the Hamiltonian (1) we have assumed the same dielectric constant $\epsilon = 7.5$ for the QW and the barrier material, whereas different values $\epsilon_{\text{QW}} \neq \epsilon_{\text{b}}$ are more realistic for experiments with thin films. The effect of the dielectric contrast has been investigated by Rytova and Keldysh [39, 40]. In Ref. [25] it has been shown that the dielectric contrast with $\epsilon_{\text{b}} < \epsilon_{\text{QW}}$ described by the RK potential causes a downshift of energies, however, the structure of energy levels is similar for both the Coulomb and the RK potential. The symmetry introduced by the quantum confinement is kept independent of the non-parabolicity of the band structure and the different dielectric constants. As a result, the avoided crossings between exciton resonances belonging to different channels, and thus the occurrence of BICs via destructive interference of these states persists. We therefore expect that BICs will be observed in future experiments on thin cuprous oxide films at quantum well widths and energies comparable with our predictions.

In conclusion, we emphasize that, although BICs have

been experimentally realized in photonics, atomic quantum systems seem to be inappropriate for their detection. Instead, we propose a Rydberg-exciton semiconductor quantum system which can, in principle, be fabricated down to lattice constant precision [28, 29]. Due to their giant exciton oscillator strengths [35] and large enough splitting of BICs and their partner states, these state pairs can be spectroscopically resolved. Here, we have rigorously shown the principal phenomenon of BIC emergence, however, more research is required to take into account all the features of the system [25, 36, 39, 40]. We believe that the experimental detection of BICs in cuprous oxide will open up ways to enhance optical nonlinearities and to improve the performance of exciton lasers [16].

ACKNOWLEDGMENTS

This work was supported by Deutsche Forschungsgemeinschaft (DFG) through the DFG Priority Programme 1929 ‘‘Giant interactions in Rydberg Systems’’ (GiRyd), Grant Nos. MA 1639/16-1 and SCHE 612/4-2.

-
- [1] C. W. Hsu, B. Zhen, A. D. Stone, J. D. Joannopoulos, and M. Soljačić, Bound states in the continuum, *Nature Reviews Materials* **1**, 16048 (2016).
 - [2] K. L. Koshelev, Z. F. Sadrieva, A. A. Shcherbakov, Y. S. Kivshar, and A. A. Bogdanov, Bound states in the continuum in photonic structures, *Physics-Uspekhi* **66**, 494 (2023).
 - [3] J. von Neumann and E. Wigner, Über merkwürdige diskrete Eigenwerte. Über das Verhalten von Eigenwerten bei adiabatischen Prozessen, *Physikalische Zeitschrift* **30**, 467 (1929).
 - [4] D. C. Marinica, A. G. Borisov, and S. V. Shabanov, Bound states in the continuum in photonics, *Phys. Rev. Lett.* **100**, 183902 (2008).
 - [5] Y. Plotnik, O. Peleg, F. Dreisow, M. Heinrich, S. Nolte, A. Szameit, and M. Segev, Experimental observation of optical bound states in the continuum, *Phys. Rev. Lett.* **107**, 183901 (2011).
 - [6] K. Koshelev, S. Kruk, E. Melik-Gaykazyan, J.-H. Choi, A. Bogdanov, H.-G. Park, and Y. Kivshar, Subwavelength dielectric resonators for nonlinear nanophotonics, *Science* **367**, 288 (2020).
 - [7] J. Wu, J. Chen, X. Qi, Z. Guo, J. Wang, F. Wu, Y. Sun, Y. Li, H. Jiang, L. Shi, J. Zi, and H. Chen, Observation of accurately designed bound states in the continuum in momentum space, *Photon. Res.* **12**, 638 (2024).
 - [8] C. Schiattarella, S. Romano, L. Sirleto, V. Mocella, I. Rendina, V. Lanzio, F. Riminucci, A. Schwartzberg, S. Cabrini, J. Chen, L. Liang, X. Liu, and G. Zito, Directive giant upconversion by supercritical bound states in the continuum, *Nature* **626**, 765 (2024).
 - [9] E. Koreshin, S. Gladyshev, I. Matchenya, R. Balafendiev, I. Terekhov, P. Belov, and A. Bogdanov, Bound States in the Continuum in a Wire Medium (2024), arXiv:2408.02089.
 - [10] F. Monticone and A. Alù, Embedded photonic eigenvalues in 3d nanostructures, *Phys. Rev. Lett.* **112**, 213903 (2014).
 - [11] E. N. Bulgakov and A. F. Sadreev, Bloch bound states in the radiation continuum in a periodic array of dielectric rods, *Phys. Rev. A* **90**, 053801 (2014).
 - [12] Z. F. Sadrieva, M. A. Belyakov, M. A. Balezin, P. V. Kapitanova, E. A. Nenasheva, A. F. Sadreev, and A. A. Bogdanov, Experimental observation of a symmetry-protected bound state in the continuum in a chain of dielectric disks, *Phys. Rev. A* **99**, 053804 (2019).
 - [13] A. F. Sadreev, Interference traps waves in an open system: bound states in the continuum, *Reports on Progress in Physics* **84**, 055901 (2021).
 - [14] L. Huang, L. Xu, D. A. Powell, W. J. Padilla, and A. E. Miroshnichenko, Resonant leaky modes in all-dielectric metasystems: Fundamentals and applications, *Physics Reports* **1008**, 1 (2023).
 - [15] F. Lei, Z. Ye, K. Twayana, Y. Gao, M. Girardi, O. B. Helgason, P. Zhao, and V. Torres-Company, Hyperparametric oscillation via bound states in the continuum, *Phys. Rev. Lett.* **130**, 093801 (2023).
 - [16] M. Kang, T. Liu, C. T. Chan, and M. Xiao, Applications of bound states in the continuum in photonics, *Nature Reviews Physics* **5**, 659 (2023).
 - [17] F. H. Stillinger and D. R. Herrick, Bound states in the continuum, *Phys. Rev. A* **11**, 446 (1975).
 - [18] H. Friedrich and D. Wintgen, Physical realization of bound states in the continuum, *Phys. Rev. A* **31**, 3964 (1985).

- [19] H. Friedrich and D. Wintgen, Interfering resonances and bound states in the continuum, *Phys. Rev. A* **32**, 3231 (1985).
- [20] L. D. Landau and L. M. Lifshitz, *Quantum Mechanics Non-Relativistic Theory, Third Edition: Volume 3* (Butterworth-Heinemann, 1981).
- [21] N. Scheuler, P. Rommel, J. Main, and P. A. Belov, Resonance energies and linewidths of Rydberg excitons in Cu_2O quantum wells, *Phys. Rev. B* **109**, 165440 (2024).
- [22] B. S. Monozon and P. Schmelcher, Resonant impurity and exciton states in a narrow quantum well, *Phys. Rev. B* **71**, 085302 (2005).
- [23] P. A. Belov, Linewidths and energy shifts of electron-impurity resonant states in quantum wells with infinite barriers, *Phys. Rev. B* **105**, 155417 (2022).
- [24] N. Moiseyev, Quantum theory of resonances: Calculating energies, widths and cross-sections by complex scaling, *Phys. Rep.* **302**, 211 (1998).
- [25] P. A. Belov, F. Morawetz, S. O. Krüger, N. Scheuler, P. Rommel, J. Main, H. Giessen, and S. Scheel, Energy states of Rydberg excitons in finite crystals: From weak to strong confinement, *Phys. Rev. B* **109**, 235404 (2024).
- [26] M. J. Seaton, Quantum defect theory, *Reports on Progress in Physics* **46**, 167 (1983).
- [27] H. Friedrich, *Theoretical Atomic Physics* (Springer, Cham, 2017).
- [28] M. Takahata, K. Tanaka, and N. Naka, Nonlocal optical response of weakly confined excitons in Cu_2O mesoscopic films, *Phys. Rev. B* **97**, 205305 (2018).
- [29] M. Takahata, K. Tanaka, and N. Naka, Superradiance-to-polariton crossover of Wannier excitons with multiple resonances, *Phys. Rev. Lett.* **121**, 173604 (2018).
- [30] A. Konzelmann, B. Frank, and H. Giessen, Quantum confined Rydberg excitons in reduced dimensions, *Journal of Physics B: Atomic, Molecular and Optical Physics* **53**, 024001 (2019).
- [31] R. Awal, N. Y. Tanisa, M. A. Rahman, and S. Ahmed, Preparation of nanostructured cuprous oxide (Cu_2O) absorber layer for photovoltaic application, *Micro & Nano Letters* **19**, e12188 (2024).
- [32] H. Fröhlich, Electrons in lattice fields, *Advances in Physics* **3**, 325 (1954).
- [33] F. Schweiner, J. Main, and G. Wunner, Linewidths in excitonic absorption spectra of cuprous oxide, *Phys. Rev. B* **93**, 085203 (2016).
- [34] P. A. Belov, Energy spectrum of excitons in square quantum wells, *Physica E: Low-dimensional Systems and Nanostructures* **112**, 96 (2019).
- [35] T. Kazimierczuk, D. Fröhlich, S. Scheel, H. Stolz, and M. Bayer, Giant Rydberg excitons in the copper oxide Cu_2O , *Nature* **514**, 343 (2014).
- [36] F. Schweiner, J. Main, M. Feldmaier, G. Wunner, and C. Uihlein, Impact of the valence band structure of Cu_2O on excitonic spectra, *Phys. Rev. B* **93**, 195203 (2016).
- [37] K. He, N. Kumar, L. Zhao, Z. Wang, K. F. Mak, H. Zhao, and J. Shan, Tightly bound excitons in monolayer WSe_2 , *Phys. Rev. Lett.* **113**, 026803 (2014).
- [38] A. Chernikov, T. C. Berkelbach, H. M. Hill, A. Rigosi, Y. Li, B. Aslan, D. R. Reichman, M. S. Hybertsen, and T. F. Heinz, Exciton binding energy and nonhydrogenic Rydberg series in monolayer WS_2 , *Phys. Rev. Lett.* **113**, 076802 (2014).
- [39] N. S. Rytova, The screened potential of a point charge in a thin film, *Moscow Uni. Phys. Bull.* **22**, 18 (1967).
- [40] L. V. Keldysh, Coulomb interaction in thin semiconductor and semimetal films, *JETP Lett.* **29**, 716 (1979).
- [41] H. Bachau, E. Cormier, P. Decleva, J. E. Hansen, and F. Martín, Applications of B-splines in atomic and molecular physics, *Reports on Progress in Physics* **64**, 1815 (2001).
- [42] Details on the construction of the diagonal and coupling potentials, the application of QDT, and calculation of the linewidths are given in the Supplemental Material [link to be inserted].
- [43] H. Feshbach, Unified theory of nuclear reactions, *Annals of Physics* **5**, 357 (1958).
- [44] K. Suzuki and J. C. Hensel, Quantum resonances in the valence bands of germanium. I. theoretical considerations, *Phys. Rev. B* **9**, 4184 (1974).
- [45] F. Schweiner, J. Main, G. Wunner, and C. Uihlein, Even exciton series in Cu_2O , *Phys. Rev. B* **95**, 195201 (2017).
- [46] J. Thewes, J. Heckötter, T. Kazimierczuk, M. Aßmann, D. Fröhlich, M. Bayer, M. A. Semina, and M. M. Glazov, Observation of high angular momentum excitons in cuprous oxide, *Phys. Rev. Lett.* **115**, 027402 (2015).
- [47] F. Schöne, S.-O. Krüger, P. Grünwald, H. Stolz, S. Scheel, M. Aßmann, J. Heckötter, J. Thewes, D. Fröhlich, and M. Bayer, Deviations of the exciton level spectrum in Cu_2O from the hydrogen series, *Phys. Rev. B* **93**, 075203 (2016).

Supplemental Material for “Bound states in the continuum in cuprous oxide quantum wells”

Angelos Aslanidis,¹ Jörg Main,^{1,*} Patric Rommel,¹ Stefan Scheel,² and Pavel A. Belov²

¹*Institut für Theoretische Physik I, Universität Stuttgart, 70550 Stuttgart, Germany*

²*Institut für Physik, Universität Rostock, Albert-Einstein-Straße 23-24, 18059 Rostock, Germany*

In this Supplemental Material, we present the derivation of the potentials $V_{nn'}(\rho)$ in Eq. (3) of the main text and explain the application of quantum defect theory (QDT) to excitons in cuprous oxide quantum wells.

I. DERIVATION OF THE DIAGONAL AND COUPLING POTENTIALS

A precise computation of the potentials $V_{nn'}(\rho)$ in the coupled-channel Schrödinger equation (2) of the main text is the prerequisite for obtaining accurate results for the bound states in the continuum (BICs) by application of quantum defect theory. The potentials (in exciton-Hartree units with $e = 4\pi\epsilon_0\epsilon = 1$) are given as

$$V_{nn'}(\rho) = V_{\{ij\},\{kl\}}(\rho) = - \int_{-L/2}^{L/2} \int_{-L/2}^{L/2} \frac{\psi_{ei}(z_e)\psi_{hj}(z_h)\psi_{ek}(z_e)\psi_{hl}(z_h)}{\sqrt{\rho^2 + (z_e - z_h)^2}} dz_e dz_h, \quad (1)$$

where $\psi_{ei}(z_e)$, $\psi_{hj}(z_h)$, $\psi_{ek}(z_e)$, and $\psi_{hl}(z_h)$ are the (analytically known) states of electron and hole in the quantum well with width L . As an example, we derive the diagonal potential $V_{11}(\rho)$, where both the electron and the hole are in the quantum well ground state, i.e.

$$\psi_{e1}(z_e) = \sqrt{\frac{2}{L}} \cos\left(\frac{\pi z_e}{L}\right), \quad \psi_{h1}(z_h) = \sqrt{\frac{2}{L}} \cos\left(\frac{\pi z_h}{L}\right). \quad (2)$$

Using the scaling $\tilde{\rho} = \pi\rho/L$, $\tilde{z}_{e,h} = \pi z_{e,h}/L$, and center and relative coordinates $Z = (\tilde{z}_e + \tilde{z}_h)/2$, $z = \tilde{z}_e - \tilde{z}_h$, we obtain

$$\begin{aligned} V_{11}(\rho) &= -\frac{4}{\pi L} \int_{-\pi}^{\pi} dz \int_{-(\pi-|z|)/2}^{(\pi-|z|)/2} dZ \frac{1}{\sqrt{\tilde{\rho}^2 + z^2}} \cos^2(Z + z/2) \cos^2(Z - z/2) \\ &= -\frac{4}{\pi L} \int_0^{\pi} dz \frac{1}{\sqrt{\tilde{\rho}^2 + z^2}} \frac{1}{8} [3 \sin(2z) + 2(\pi - z)(\cos(2z) + 2)] \\ &\stackrel{z \equiv \tilde{\rho}x}{=} -\frac{1}{2\pi L} \int_0^{\pi/\tilde{\rho}} dx \frac{1}{\sqrt{1+x^2}} [3 \sin(2\tilde{\rho}x) + 2(\pi - \tilde{\rho}x)(\cos(2\tilde{\rho}x) + 2)]. \end{aligned} \quad (3)$$

The remaining integral cannot be solved analytically. We now consider two cases, viz. the regions $\rho \gtrsim 1.5L$ and $\rho \lesssim 1.5L$. For $\rho \gtrsim 1.5L$, i.e., large values $\tilde{\rho} \gtrsim 1.5\pi$, the values of x in Eq. (3) are restricted to $|x| < 1$, and thus the Taylor series

$$\frac{1}{\sqrt{1+x^2}} = 1 - \frac{1}{2}x^2 + \frac{3}{8}x^4 - \frac{5}{16}x^6 + \frac{35}{128}x^8 \mp \dots \quad (4)$$

converges. Inserting this series into Eq. (3) the integrals of all individual terms can now be solved analytically providing the asymptotic formula valid for $\rho \gtrsim 1.5L$

$$V_{11}(\rho) = - \sum_{n=0}^{n_{\max}} c_n \frac{L^{2n}}{\rho^{2n+1}} \quad (5)$$

with in principle analytically known coefficients, see Table I. We used $n_{\max} = 10$ in our computations. For $\tilde{\rho} \lesssim 1.5\pi$

* Email: main@itp1.uni-stuttgart.de

TABLE I. Coefficients of the asymptotic expansion (5) of the diagonal potential $V_{11}(\rho)$.

c_0	1
c_1	-0.03267274151216445
c_2	0.004328401188903151
c_3	-0.0009619175433854251
c_4	0.0002864777243269292
c_5	-0.0001035053259902042
c_6	0.0000429546345632382
c_7	-0.00001979479166677419
c_8	$9.903495293081103 \times 10^{-6}$
c_9	$-5.294507909335873 \times 10^{-6}$
c_{10}	$2.98956638899579 \times 10^{-6}$

the evaluation of Eq. (3) is less straightforward. When writing

$$V_{11}(\rho) = -\frac{1}{2\pi L} \int_0^{\pi/\tilde{\rho}} dx \frac{f(x)}{\sqrt{1+x^2}} \quad (6)$$

the function $f(x) = 3 \sin(2\tilde{\rho}x) + 2(\pi - \tilde{\rho}x)(\cos(2\tilde{\rho}x) + 2)$ can be expanded in terms of Legendre polynomials, transformed from the standard interval $[-1, 1]$ to the range $[0, \pi/\tilde{\rho}]$. For $f(x)$ given as a polynomial, the integral in Eq. (6) can be solved analytically. Using Legendre polynomials up to order six yields the expansion

$$V_{11}(\rho) = -\frac{1}{L} \left[d_1 \frac{\rho}{L} + d_3 \frac{\rho^3}{L^3} + d_5 \frac{\rho^5}{L^5} + \left(d_0 + d_2 \frac{\rho^2}{L^2} + d_4 \frac{\rho^4}{L^4} \right) \sqrt{1 + \rho^2/L^2} \right. \\ \left. + \left(e_0 + e_2 \frac{\rho^2}{L^2} + e_4 \frac{\rho^4}{L^4} + e_6 \frac{\rho^6}{L^6} \right) \operatorname{arcsinh} \left(\frac{L}{\rho} \right) \right] \quad (7)$$

with coefficients d_i and e_i . This expansion is valid for $\rho \lesssim 1.5L$. Note that contrary to the asymptotic formula (5) the coefficients in Eq. (7) are not unique but depend on the order of the expansion. We used symbolic calculations with Wolfram Mathematica [1] for the evaluation of Eq. (3) and the computation of the coefficients in Eqs. (5) and (7).

When the ground state wave functions (2) for the electron and hole in the quantum well are replaced in Eq. (1) with appropriate excited states $\psi_{ei,hj}(z_{e,h})$, similar expansions as Eqs. (5) and (7) for $V_{11}(\rho)$ can be derived for other coupling potentials $V_{nn'}(\rho) = V_{\{ij\},\{kl\}}(\rho)$ with $n > 1$, $n' > 1$, which are shown in Fig. 2 of the main text. The leading coefficient in Eq. (5) is $c_0 = 1$ in case of the diagonal potentials and $c_0 = 0$ in case of the non-diagonal coupling potentials. This leads to the asymptotic behavior of the potentials for large values of ρ as discussed in the main text.

II. APPLICATION OF QUANTUM DEFECT THEORY

When applying QDT to cuprous oxide excitons in quantum wells, we only consider the three lowest even-parity channels formed by quantum-confinement quantum numbers $(n_e, n_h) = (1, 1)$ for the first channel ($n = 1$), and $(n_e, n_h) = (3, 1)$ and $(2, 2)$ for the second ($n = 2$) and third ($n = 3$) channels, respectively. The restriction to only three channels is justified by the fact that the threshold of the fourth even-parity channel with quantum numbers $(n_e, n_h) = (1, 3)$ is energetically well separated from the three lower thresholds for quantum well widths $L \lesssim 20$ nm. In a first step we solve the Schrödinger equation (2) in the main text by considering only the diagonal potentials $V_{nn}(\rho)$. In a second step, the lowest 10 eigenstates in each channel are then taken to set up an eigenvalue problem by including the nondiagonal coupling potentials $V_{nn'}(\rho)$. The linewidths of the states obtained by the three-channel QDT are computed by the Feshbach formula, see below. Finally, we search for states with vanishing linewidths, viz. the bound states in the continuum (BICs).

A. One-channel QDT

The wave functions $\Phi_n^N(\rho)$ with principal quantum number N in the even-parity channel n described by the diagonal potential $V_{nn}(\rho)$ and threshold energy E_n are solutions of the one-channel quantum-defect Schrödinger equation

$$\left[E_n - \frac{\hbar^2}{2\mu} \left(\frac{\partial^2}{\partial \rho^2} + \frac{1}{\rho} \frac{\partial}{\partial \rho} - \frac{m^2}{\rho^2} \right) + V_{nn}(\rho) \right] \Phi_n^N(\rho) = E_n^N \Phi_n^N(\rho). \quad (8)$$

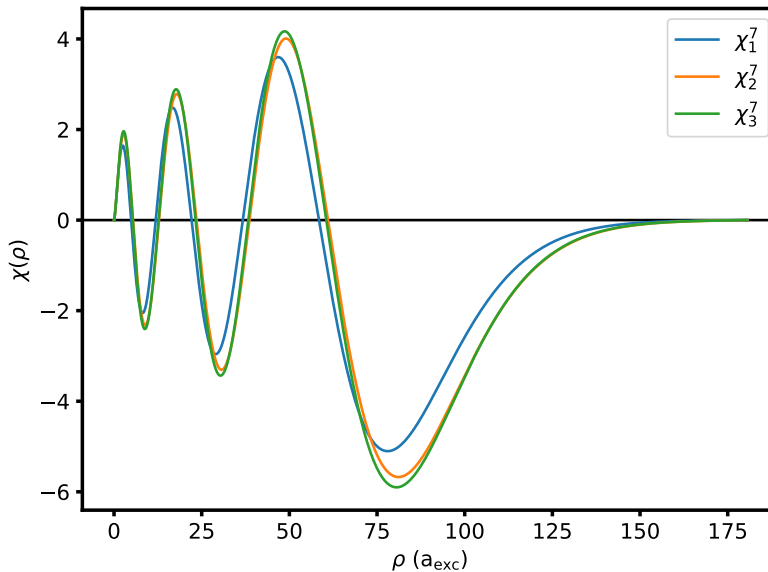


FIG. 1. One-channel QDT wave functions $\chi_n^N(\rho) = \sqrt{\rho}\Phi_n^N(\rho)$ with angular quantum number $m = 1$ and principal quantum number $N = 7$ in the even-parity channels $n = 1$ to 3. a_{exc} is the exciton Bohr radius.

They are obtained by numerical integration of the wave function with initial conditions

$$\Phi_n^N(\rho_0) = \rho_0^{|m|}, \quad \frac{d}{d\rho}\Phi_n^N(\rho_0) = |m|\rho_0^{|m|-1} \quad (9)$$

at a small value of ρ_0 to fulfill the boundary condition $\Phi_n^N(\rho) \sim \rho^{|m|}$ in the limit $\rho \rightarrow 0$. Here, m is the magnetic quantum number. To also fulfill the boundary condition $\Phi_n^N(\rho) = 0$ for $\rho \rightarrow \infty$, a numerical root search is applied by varying the energy $E = -E_{\text{Ryd}}/N_{\text{eff}}^2$, with the effective quantum numbers $N_{\text{eff}} = N - \delta_N$ and the quantum defects δ_N . For illustration, the one-channel QDT wave functions $\chi_n^N(\rho) = \sqrt{\rho}\Phi_n^N(\rho)$ with angular quantum number $m = 1$ and principal quantum number $N = 7$ in the even-parity channels $n = 1$ to 3 are shown in Fig. 1.

B. Three-channel QDT

The wave functions $\Phi_n^N(\rho)$ with the magnetic quantum number $m = 1$ and the principal quantum numbers $N = 2$ to 11 in the three lowest even-parity channels ($n = 1, 2, 3$) are taken as a basis for the expansion

$$\Psi_n(\rho) = \sum_N c_n^N \Phi_n^N(\rho) \quad (10)$$

of the solution of the coupled-channel Schrödinger equation (2) in the main text. The nondiagonal matrix elements of the (30×30) -dimensional Hamiltonian matrix are obtained by numerical integration using the coupling potentials $V_{nn'}(\rho)$ with $n \neq n'$ and the wave functions $\Phi_n^N(\rho)$ of the three lowest channels. The Hamiltonian matrix is diagonalized with a conventional linear algebra routine to obtain the energy eigenvalues presented in Figs. 3 and 4 of the main text. The coefficients c_n^N of the eigenvectors of the (30×30) -dimensional Hamiltonian matrix can be used to expand the final wave functions Ψ as solution of the coupled-channel Schrödinger equation (2) in the main text in terms of the one-channel QDT basis functions $\Phi_n^N(\rho)$.

C. Computation of the linewidths

The linewidths of resonances in the energy region with one open channel ($E_1 < E < E_2$) are given by the Feshbach formula [2, 3]

$$\Gamma = 2\pi|\langle\Phi_1|V_{12}\Psi_2 + V_{13}\Psi_3\rangle|^2, \quad (11)$$

where $(\Psi_2, \Psi_3)^T$ is a part of the solution of the three-channel Schrödinger equation associated with the two closed channels. The energy normalized regular scattering wave function $\Phi_1(\rho)$ in the open channel ($n = 1$) is obtained by numerical integration of the wave function with the initial conditions (9) and is adjusted to the asymptotic form [4]

$$\Phi_1^{\text{asy}}(\rho) = \frac{1}{\sqrt{\hbar\pi}} \left(\frac{2m}{E} \right)^{1/4} \frac{1}{\sqrt{\rho}} \sin \left(k\rho + \frac{1}{k} \ln(2k\rho) - \pi/2 + \delta(k) \right), \quad (12)$$

where $\delta(k)$ is a phase shift and $k = \sqrt{2mE/\hbar^2}$, to guarantee proper normalization. Using Eq. (10) for the expansion of the wave function Ψ in terms of the one-channel QDT basis functions $\Phi_n^N(\rho)$, the overlap matrix elements in Eq. (11) are obtained as

$$\langle \Phi_1 | V_{12} \Psi_2 + V_{13} \Psi_3 \rangle = \sum_N [c_2^N \langle \Phi_1 | V_{12} | \Phi_2^N \rangle + c_3^N \langle \Phi_1 | V_{13} | \Phi_3^N \rangle] . \quad (13)$$

A vanishing overlap matrix element (13) at a certain width L of the quantum well, due to destructive interference of the wave functions in the two closed channels, characterizes a BIC. When the basis of one-channel QDT wave functions for the matrix setup is restricted to only one state in each of the two closed channels, which undergo an avoided crossing when the QW width L is varied, the energy eigenvalues, linewidths, and the condition for the occurrence of a BIC are obtained analytically as described in the main text.

-
- [1] Wolfram Research, Inc., Mathematica.
 - [2] H. Feshbach, Unified theory of nuclear reactions, *Annals of Physics* **5**, 357 (1958).
 - [3] H. Friedrich, *Theoretical Atomic Physics* (Springer, Cham, 2017).
 - [4] L. D. Landau and L. M. Lifshitz, *Quantum Mechanics Non-Relativistic Theory, Third Edition: Volume 3* (Butterworth-Heinemann, 1981).